Locking of periodic patterns in Cahn-Hilliard models for Langmuir-Blodgett transfer

Markus Wilczek* and Svetlana V. Gurevich
Institute for Theoretical Physics, University of Münster, Wilhelm-Klemm-Straße 9, 48149 Münster, Germany
(Received 24 July 2014; published 29 October 2014)

The influence of a periodic spatial forcing on the pattern formation in a generalized Cahn-Hilliard model describing Langmuir-Blodgett transfer is studied. The occurring locking effects enable a control mechanism for the pattern formation process. In the one-dimensional case the parameter range in which patterns are created is increased and the patterns' properties can be adjusted in a broader range. In two dimensions, one-dimensional stripe patterns can be destabilized, giving rise to a multitude of complex two-dimensional structures, including oblique and lattice patterns.

DOI: 10.1103/PhysRevE.90.042926 PACS number(s): 05.45.Xt, 81.16.Rf, 68.18.Jk

I. INTRODUCTION

Locking and synchronization phenomena are ubiquitous in diverse areas, starting from physiological systems such as oscillators in the human body [1,2] to technical applications such as chaotic pulsed lasers, magnetic nano-oscillators, or modern power grids [3–5]. A rather beneficial utilization of synchronization and locking effects is the control of pattern formation processes. While such systems exhibit natural spatial and temporal frequencies, they can be entrained to an external forcing, providing an additional control mechanism. Although the term synchronization is more commonly known in the context of temporal oscillations, there are numerous systems where spatial patterns exhibit wave-number locking to an external spatial forcing, similar to temporal synchronization, e.g., in spatially forced chemical systems [6] or convection [7–9]. Extensive theoretical studies have also been made in the context of Turing patterns [10], a Ginzburg-Landau type of equation [11], Swift-Hohenberg equations [12], and phase separation phenomena [13,14]. Among others, the control via locking effects can be utilized in coating processes with thin layers [15,16]. The coverage of substrates with thin layers of organic molecules finds various applications today, for example, in the creation of sensor devices [17] or organic transistors and light-emitting diodes [18]. The employment of self-organization phenomena for the creation of such thin layers facilitates the production of structured layers [19,20]. The effective use of self-organization phenomena of course necessitates extensive control over the whole process. One of the common methods to control pattern formation processes is the use of prestructures that enable locking effects to occur [21–25]. If these effects are robust, the requirements regarding the accuracy of the rest of the process are lower and therefore in practice more easily achievable.

Here we are interested in a description of locking effects in a generalized Cahn-Hilliard model [26] that was introduced to describe self-organized patterns arising by Langmuir-Blodgett (LB) transfer [20,27] onto prestructured substrates. The experimental setup for LB transfer consists of a trough filled with water, on which a floating monolayer of amphiphilic molecules, such as dipalmitoylphosphatidylcholine, is prepared (see Fig. 1, left panel). A substrate is then pulled out of the trough, leading to a transfer of the floating monolayer onto the substrate. Movable barriers on the surface of the water are used to keep the area density of the monolayer constant, even if molecules are carried away on the substrate. As the monolayer is confined to the surface of the water, it constitutes a truly two-dimensional gas or liquid. The phase of the monolayer depends on its density and can therefore be controlled by the movable barriers. In the experiments that we are interested in [20,28,29], the monolayer is in a low-density liquid-expanded (LE) phase. However, during the transfer, the monolayer is subject to a short-range interaction with the substrate, the so-called substrate-mediated condensation (SMC) [29–32]. This effect lowers the coexistence pressure of the LE phase with the more dense liquid-condensed (LC) phase in the vicinity of the substrate. Therefore, a phase transition of the monolayer into the LC phase is energetically favored as soon as it is transferred onto the substrate. This is experimentally observed if the substrate is pulled out of the trough sufficiently slow. For higher transfer velocities, however, the condensation of the monolayer does not occur uniformly but periodically, leading to the transfer of patterns consisting of domains in the LC phase alternating with domains in the LE phase. The patterns that can be obtained are highly regular stripe and lattice patterns [20]. As a main control parameter, the transfer velocity determines the type of pattern and its properties such as wavelength and orientation.

A way to gain more control over the pattern formation process is the use of prestructured substrate. In the following, we will consider substrates that have a periodic prestructure, which means that certain properties of the substrate vary with a well defined spatial frequency. This introduces a periodic forcing, which can change the properties of the generated patterns, depending on, e.g., the strength of the forcing. This in turn is related to the contrast of the prepattern, i.e., how strong a certain property of the substrate varies along the prestructure. If the contrast is strong enough, the pattern formation process locks to the prestructure, resulting in a perfect control over the produced structures.

This paper is organized as follows. Section II contains a derivation of the generalized Cahn-Hilliard model. In Sec. III the results of this model in the case of a transfer onto homogeneous substrates are briefly discussed. The results for the transfer onto prestructured substrates are presented in Sec. IV for the one-dimensional case and in Sec. V for the two-dimensional case.

*markuswilczek@uni-muenster.de

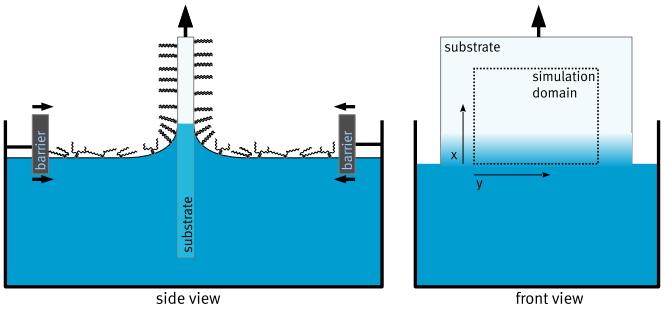

FIG. 1. (Color online) Shown on the left is a sketch of the experimental setup for Langmuir-Blodgett transfer. A substrate is pulled out of a trough filled with water, on which a floating monolayer of amphiphilic molecules is prepared. Movable barriers compress the monolayer during the transfer to keep the area density constant. Shown on the right is the front view illustrating the frame of reference and the coordinate system used in the numerical simulations.

II. MODEL EQUATIONS

Since the monolayer is in a stable LE phase before the transfer, the formation of domains in the LC phase can only occur in the vicinity of the substrate. Therefore, the relevant part of the experiment that needs to be described by a theoretical model is confined to the meniscus, where the water layer between the monolayer and the substrate becomes thin. Under this assumption, the transfer process can be well described by the dynamics of the water layer in a lubrication approximation [33] coupled to the dynamics of the floating monolayer on its surface [34,35]. Such a model has been developed in [36] and proven to be able to describe most phenomena occurring during Langmuir-Blodgett transfer onto homogeneous substrates, as well as onto prestructured substrates [25]. However, the results of this model indicate that the dynamics of the water layer only has a minor impact on the pattern formation process, which is dominated by the dynamics of the floating monolayer undergoing a phase decomposition. Therefore, a reduced model can be derived, in which the water layer is assumed to be static and its shape only enters parametrically [26]. The evolution equation for the density of the monolayer then has the form of a generalized Cahn-Hilliard equation. While in [26] such a model has been presented on the basis of the full thin-film model, here we introduce the model starting from the general Cahn-Hilliard equation [37] and introducing the contributions specific to the case of LB transfer. It has to be emphasized that, while this minimal theoretical model for LB transfer has proven to be able to capture the main features of pattern formation occurring in the experiments, we do not intend to make quantitative predictions. Therefore, we do not give a specific scaling of the dimensionless quantities used in the equation and also do not derive parameters from experimental data. In contrast, we want to facilitate the comparison of the results with results obtained in similarly general models, such as in the Swift-Hohenberg equation [12] or in reaction-diffusion systems [6].

The Cahn-Hilliard equation for the concentration $c(\mathbf{x},t)$ of the monolayer in one ($\mathbf{x} = x \in \Omega_1 \subset \mathbb{R}$) or two [$\mathbf{x} = (x,y) \in \Omega_2 \subset \mathbb{R}^2$] dimensions reads

$$\frac{\partial}{\partial t}c(\mathbf{x},t) = \nabla \cdot \left(M \nabla \frac{\delta F(c)}{\delta c} \right), \tag{1}$$

with the mobility M and the free energy $F(c)$ given by

$$F(c) = \int \frac{1}{2}(\nabla c)^2 - \frac{1}{2}c^2 + \frac{1}{4}c^4 + \mu\zeta(\mathbf{x})c \, d\mathbf{x}. \tag{2}$$

The free energy (2) includes the Cahn-Hilliard contribution due to spatial inhomogeneities [38] and a double-well approximation for the free energy of the uniform system, which is justified in the vicinity of the LE-LC phase transition of the monolayer [36]. Here μ is a coefficient regulating the strength of the SMC, which is spatially varying with the function $\zeta(\mathbf{x})$. For $\mu = 0$ the two minima of the free energy $c = \pm 1$ have equal depth and correspond to a monolayer in the pure LE phase ($c = -1$) or in the pure LC phase ($c = +1$). For $\mu > 0$ the double well of the free energy has a skewness favoring the LC phase. The form of $\zeta(\mathbf{x})$ reflects the characteristics of the liquid layer between the monolayer and the substrate located at the meniscus. Here we use the form

$$\zeta(\mathbf{x}) = -\frac{1}{2}\left[1 + \tanh\left(\frac{x - x_s}{l_s}\right)\right], \tag{3}$$

which ensures a smooth transition from no influence of the SMC [$\zeta(\mathbf{x}) = 0$] before the meniscus ($x < x_s$) to a fixed value [$\zeta(\mathbf{x}) = -1$] after the meniscus ($x > x_s$), which is located at x_s. The width of the transition region is determined by l_s. While we will use the hyperbolic tangent shape in the following, the concrete shape of $\zeta(\mathbf{x})$ only has a minor impact on the simulations.

The transfer process is included into the model through an additive advective term $\mathbf{v} \cdot \nabla c$ with the transfer velocity $\mathbf{v} = (v,0)$. Incorporating these contributions and assuming the mobility to be constant ($M = 1$), the final model reads

$$\frac{\partial}{\partial t}c(\mathbf{x},t) = \nabla \cdot \{\nabla[-\Delta c - c + c^3 + \mu\zeta(\mathbf{x})] - \mathbf{v}c\}. \tag{4}$$

This equation is solved numerically on a one- or two-dimensional domain ($\Omega_1 = [0,L]$ and $\Omega_2 = [0,L] \times [0,L]$, respectively) with the boundary conditions

$$c|_{x=0} = c_0, \quad \left.\frac{\partial}{\partial x}c\right|_{x=L} = 0, \quad \left.\frac{\partial^2}{\partial x^2}c\right|_{x=0,L} = 0, \tag{5}$$

$$c|_{y=0} = c|_{y=L}. \tag{6}$$

The boundary at $x = 0$ reflects the role of the Langmuir-Blodgett trough supplying a constant density c_0 of the monolayer on the surface of the water and therefore in front of the meniscus. Ideally, the boundary at $x = L$ should not influence the outflow of the concentration c with $\mathbf{v}$, which is hard to realize. However, the conditions given in (5) are nearly nonreflective, restricting the region of their impact close to the boundary. On a sufficiently large simulation domain, the influence on the region of interest can therefore be safely neglected. The boundary conditions in the y direction (6) are chosen to be periodic in two-dimensional simulations [see Fig. 1 (right panel) for a clarification of the coordinate system]. The simulations were performed using an adaptive Runge-Kutta 4(5) time-integration scheme with time steps

of order 10^{-2}–10^{-1} and finite-difference evaluations of the spatial derivatives on a grid of 500 (384×384 in two dimensions) points. The methods were implemented using the NVIDIA CUDA framework [39] for computations on graphics processors.

III. TRANSFER ONTO HOMOGENEOUS SUBSTRATES IN ONE DIMENSION

The transfer onto a homogeneous substrate in one dimension has already been discussed in detail in [26,40]. We briefly summarize the most important findings here to enable an easier comparison with the results on prestructured substrates in the following section. In [26], four stable solution types of (4) and (5) have been identified: two solution types corresponding to the transfer of a homogeneous LC layer for low velocities, one solution type corresponding to a homogeneous LE layer for high velocities, and one solution type corresponding to stripes of alternating LE and LC domains parallel to the meniscus for intermediate velocities. These results, which can be obtained by direct numerical simulations, are shown in Fig. 2. Each solution type corresponds to a branch in a diagram where the L^2 norm of the solutions is plotted against the transfer velocity. In [26], such a diagram was augmented by unstable stationary solutions, which were traced using continuation methods, resulting in a complete bifurcation diagram for the one-dimensional system. In this diagram, the unstable stationary solutions exhibit a heteroclinic snaking behavior connecting the stable stationary solutions corresponding to homogeneous LE and LC layer transfers. One of the unstable solution branches is also connected to the stable LE branch by the branch corresponding to the periodic solutions (Fig. 2, blue line) generating stripes parallel to the meniscus. This branch emerges in a homoclinic bifurcation at low velocities, while at high velocities it ceases in a sequence of subcritical Hopf bifurcations.

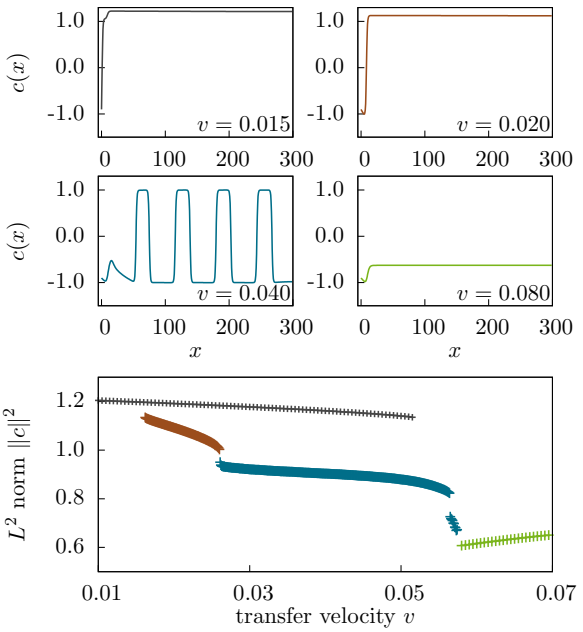

FIG. 2. (Color online) Overview of stable stationary and periodic solutions of (4) and (5) in one dimension (bottom panel). The solution types are shown as branches in an $L^2 = \|c(x)\|^2 := [\frac{1}{L}\int_0^L c(x)^2 dx]^{1/2}$ versus v diagram. For each branch an exemplary solution is shown (four top panels).

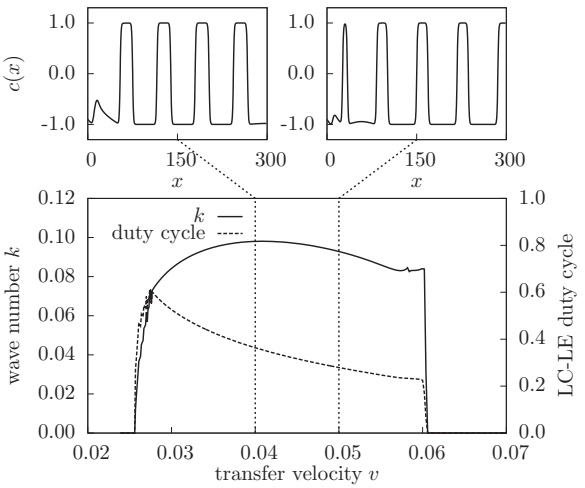

FIG. 3. Wave number k (solid line) and duty cycle (dashed line) of generated patterns during a transfer onto a homogeneous substrate in one dimension, dependent on the transfer velocity v for $c_0 = -0.9$ (bottom). Two snapshots of exemplary solutions for $v = 0.04$ and 0.05 are shown (top).

To be able to discuss the influence of prestructured substrates on the dynamics of periodic solutions, we will start with a discussion of the properties of the one-dimensional case of a transfer onto a homogeneous substrate, where the generated pattern can be characterized by the wave number k and the duty cycle, i.e., the ratio between the width of the stripes in the LC phase and the wavelength. The dependence of the wave number k and the duty cycle on the transfer velocity v is shown in Fig. 3. Up to a certain threshold velocity, a homogeneous layer in the LE phase is transferred. Above this threshold, domains in the LC phase alternating with domains in the LE phase arise at the location of the meniscus and are then carried away with the transfer velocity v. That is, temporal oscillations of the concentration at the meniscus translate to the resulting spatial patterns on the substrate. At the onset of pattern formation, the wave number k steeply increases with v up to a maximum for intermediate transfer velocities after which the wave number decreases again. Therefore, patterns with the same wave number are created for different velocities. The patterns are not identical, however, because the duty cycle of the generated pattern is monotonically decreasing with increasing speed. Above a certain threshold velocity, a homogeneous layer in the LC phase is transferred, corresponding to $k = 0$. We define the velocity interval between these threshold velocities as the patterning regime. At the upper limit of the patterning regime, the location where new stripes are formed is carried further and further into the domain and the patterning regime therefore ends as soon as this location is outside the simulation domain. The upper threshold velocity is therefore dependent on the actual domain size.

Besides the transfer velocity, also the boundary value c_0 of the concentration is an important control parameter influencing the pattern formation process. The dependence of the wave

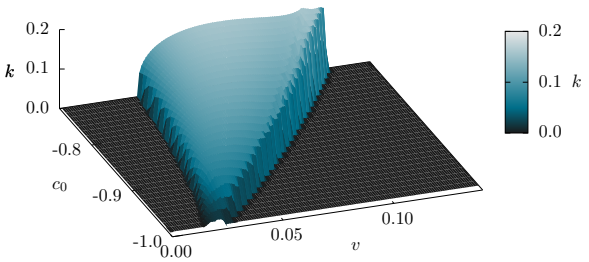

FIG. 4. (Color online) Wave number k of generated patterns during a transfer onto a homogeneous substrate in one dimension, dependent on the transfer velocity v and the boundary concentration value c_0. The patterning regime broadens and shifts towards higher velocities for increasing c_0.

number k in the patterning regime on the transfer velocity v and the boundary concentration c_0 is shown in Fig. 4. One can clearly see that the patterning regime broadens and shifts towards higher velocities v for increasing c_0. Without loss of generality, $c_0 = -0.9$ will be used for the following discussion.

IV. LOCKING TO PERIODIC PRESTRUCTURES IN ONE DIMENSION

In general, two different types of prestructures can be distinguished. Topological prestructures consist of the same material as the underlying substrate and are defined by the spatially varying height profile. In contrast, chemically prestructured substrates have a flat profile but another property that is spatially varying, e.g., the wettability. In experiments, both types often occur simultaneously, when prestructures made of a material different from the substrate are used, e.g., gold stripes on a silicon substrate. As we assume no dynamics of the liquid layer in our model (4) and (5), only the varying interaction of the monolayer with the substrate has to be included, which is connected to the disjoining pressure [41,42]. Therefore, one can model the prestructure via a spatial modulation $m(\mathbf{x},t)$ of the strength $\zeta(\mathbf{x})$ of the SMC,

$$\zeta(\mathbf{x}) = -\frac{1}{2}\left[1 + \tanh\left(\frac{x - x_s}{l_s}\right)\right][1 + \rho m(\mathbf{x},t)]. \quad (7)$$

The form of the function $m(\mathbf{x},t)$ mimics the form of the prestructure. For stripes that are parallel to the meniscus we use

$$m(\mathbf{x},t) = \tanh\left\{10\left[4\left|\mathrm{frac}\left(\frac{x - vt}{L_{\mathrm{pre}}}\right) - 0.5\right| - 1\right]\right\}. \quad (8)$$

This delivers a kink-antikink train with periodicity L_{pre}, where the steepness of the kinks is determined by the constant 10 and frac denotes the fractional part of the argument. The strength of the prestructure is determined by the contrast ρ. A sketch of a resulting strength $\zeta(x)$ of the SMC in one dimension is shown in Fig. 5. Note that the prestructure is fixed to the substrate and therefore also moves with a velocity v in the reference frame.

The resulting model (4)–(8) is a spatially forced Cahn-Hilliard equation, which has strong similarities to studies from the literature [13,14,43]. In [13], a uniformly quenched

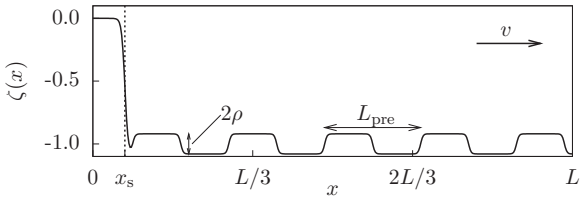

FIG. 5. Sketch of the spatial dependence of $\zeta(x)$ defined by Eqs. (7) and (8) for a prestructured substrate, indicating the local strength of the SMC. The sketch is only a snapshot as the prestructure moves with the velocity v to the right.

Cahn-Hilliard model influenced by a resting spatial forcing was studied, while in [14] a Cahn-Hilliard model subject to a moving quenching front was discussed. In the latter, also a modulation of the quenching front position was included. An extension of [13] towards a moving spatial forcing was presented in [43]. The model (4)–(8) incorporates aspects of all the work mentioned, as the pattern formation occurs at a fixed front defined by the onset of SMC at $x = x_s$ and is influenced by a moving spatial forcing, while the whole system is also subject to an advection. Although similar, the front in the model (4)–(8) is not equal to the quenching front present in [14,43]. A quenching front typically describes the transition from a one-phase (single-well potential) to a two-phase (double-well potential) region, while the front used here is a transition from a symmetric double-well potential to a tilted double-well potential. Additionally, the fixed front in combination with the advection is a crucial aspect of this model, as it selects a distinct wavelength of the emerging pattern, in contrast to a classical Cahn-Hilliard model, where no distinguished wavelength exists. That is, the pattern formation process in the case described here is driven by the concentration oscillations at the meniscus, which are subject to the moving prestructure, creating a temporal periodic forcing. Therefore, one can think of the occurring patterns as the result of a synchronization process.

In contrast to the work presented in [26], we now investigate the transfer onto a prestructured substrate and therefore a nonvanishing contrast $\rho \neq 0$. In this case the k versus v curve changes by exhibiting jumps to plateaus that correspond to a wave number commensurable with the wave number of the prestructure k_{pre}. These plateaus grow with increasing contrast ρ, as can be seen in Fig. 6. Within these plateaus, the generated pattern is almost independent of the transfer velocity, which can reduce the necessary accuracy of the transfer velocity control in the experimental system. In addition, the use of a prestructured substrate extends the velocity range in which periodic structures are generated towards higher transfer velocities and extends the wave-number range that is accessible towards higher wave numbers, i.e., smaller wavelengths, which can be seen at the 1:1 locking plateau. Both effects enable the production of a broader range of patterns at a larger range of experimental parameters. Note that the wave numbers k plotted in Fig. 6 are averaged over time, because for higher-order locking ratios, such as 2:3, the resulting pattern can consist of alternating stripes with different periodicities, which only on average are commensurable with the prestructure periodicity.

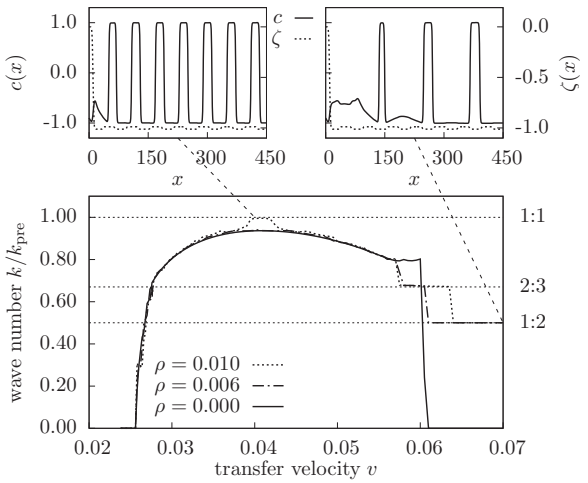

FIG. 6. Wave number k of generated patterns during a transfer onto a prestructured substrate in one dimension, dependent on the transfer velocity v and the prestructure contrast ρ of a prestructured substrate with $L_{\text{pre}} = 60$ (bottom). Two snapshots of exemplary solutions for $v = 0.04$ and 0.07 (both at $\rho = 0.01$) are shown (solid lines, top), indicating 1:1 and 1:2 locking with the prestructure (dotted lines, top).

A good overview of the possible locking regimes can be gained in an Arnold tongue diagram [2], where the parameter regions in which locking effects occur are marked as colored areas in the ρ-v plane, with each color referring to a different locking ratio (see Fig. 7). Of course the structure of such a diagram also depends on the periodicity of the prestructure, as can be seen in the comparison of the Arnold diagrams for a prestructure wavelength of $L_{\text{pre}} = 60$ (top) and $L_{\text{pre}} = 240$ (bottom). However, common features can be identified, such as the shape of the 1:2 locking tongue in the $L_{\text{pre}} = 60$ diagram and the 2:1 locking tongue in the $L_{\text{pre}} = 240$ diagram, which both correspond to stripes with a periodicity of $\lambda = 120$.

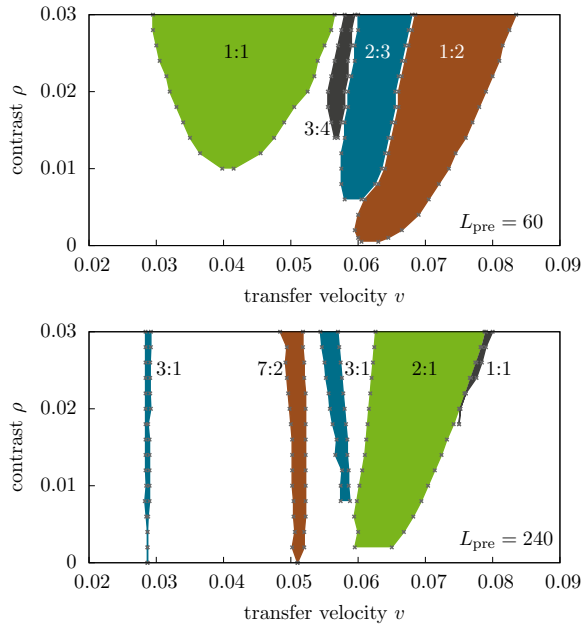

FIG. 7. (Color online) Arnold tongue diagrams showing the locking regimes depending on transfer velocity and prestructure contrast, where different colors correspond to different locking ratios. The crosses depict the boundaries of the locking regimes. The wavelength of the prestructure is $L_{\text{pre}} = 60$ (top) and $L_{\text{pre}} = 240$ (bottom), corresponding to a wave number $k_{\text{pre}} = \frac{2\pi}{L_{\text{pre}}} \approx 0.105$ (top) and $k_{\text{pre}} \approx 0.026$ (bottom).

Despite obvious quantitative differences, the results obtained in the model (4)–(8) are similar to the results obtained in the full two-component model for the Langmuir-Blodgett transfer presented in [25]. Both models predict the existence of similarly shaped locking regimes for various locking ratios at a broad range of transfer velocities and prestructure contrasts. The feature of increasing locking domains for increasing prestructure contrast ρ is also common to both models. The fact that this model resembles the findings in the full two-component model additionally clarifies the origin of the locking effects to be the interaction of the prestructure and the surfactant monolayer, while the interaction of the prestructure and the liquid layer seems to have a minor impact. The similarity of the results also further justifies the use of the simplified model employed here, as it proofs that it still captures the important physical effects even for prestructured substrates.

V. EFFECTS OF PERIODIC PRESTRUCTURES IN TWO DIMENSIONS

The stable solution types of the one-dimensional system, i.e., homogeneous transfer of LE layers, alternating stripes in the LE and LC phase parallel to the meniscus, and homogeneous transfer of LC layers, are also solutions of the two-dimensional system (4)–(6) if they are only extended homogeneously in the new spatial y direction [26]. Furthermore, for low transfer velocities within the patterning regime, stripes parallel to the meniscus are unstable and stripes perpendicular to the meniscus are created and transferred. Due to the periodic boundary conditions in the y direction, sometimes defects in the stripe pattern occur if the natural wavelength of the pattern does not fit the periodicity of the simulation domain. See Fig. 8 for an overview of the possible two-dimensional basic pattern types.

Considering prestructured substrates in two dimensions, the results from the one-dimensional system can be directly reproduced by using stripes parallel to the meniscus as a prestructure. Snapshots of numerical solutions for different

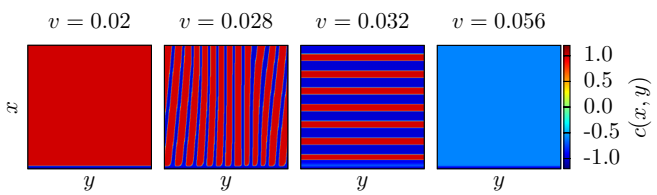

FIG. 8. (Color online) Overview of basic pattern types in two dimensions on homogeneous substrates ($\rho = 0, L = 600$). The meniscus is located at the bottom of the snapshots, with the transfer direction going from bottom to top. The patterns correspond to a homogeneous LC transfer, stripes perpendicular to the meniscus, stripes parallel to the meniscus, and a homogeneous LE transfer (from left to right).

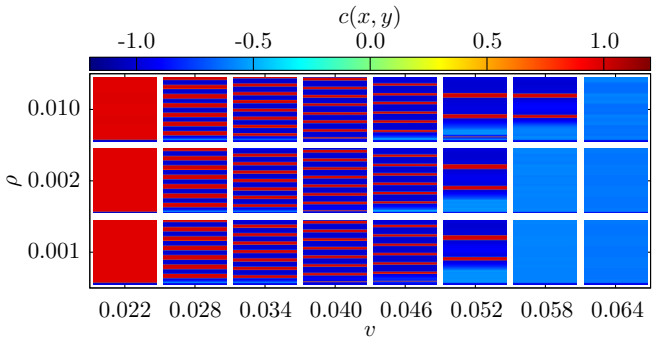

FIG. 9. (Color online) Overview of occurring patterns on a prestructured substrate with stripes parallel to the meniscus with $L_{\text{pre}} = 200$.

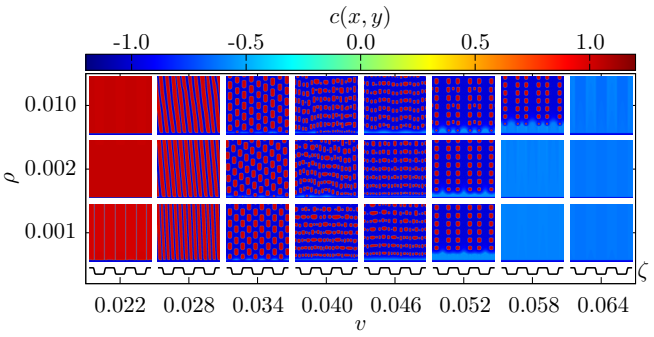

FIG. 10. (Color online) Overview of occurring patterns on a prestructured substrate with stripes perpendicular to the meniscus with $L_{\text{pre}} = 200$. A schematic cross section of the prestructure is shown below the solution panels. The possible patterns comprise stripes with different orientations as well as regular and irregular lattice structures.

transfer velocities v and prestructure contrasts ρ are shown in Fig. 9, where only solutions homogeneous in the y direction occur. This means that stripes parallel to the meniscus are further stabilized by a prestructure with stripes parallel to the meniscus [44]. This is particularly important in the lower-velocity part of the patterning regime, where a transfer onto a homogeneous substrate would result in stripes perpendicular to the meniscus. That is, the instability leading to this solution type is suppressed by the use of a prestructured substrate. Interestingly, there also exist small parameter regimes (e.g., $v = 0.038, \rho = 0.01$, not shown) where the pseudo-one-dimensional patterns are not further stabilized by a pseudo-one-dimensional prestructure but are in fact destabilized, so the stripes parallel to the meniscus break up into smaller domains, which are still roughly aligned in lines. This is reminiscent of similar results found in the Swift-Hohenberg equation [12], where a pseudo-one-dimensional forcing can also destabilize equally aligned stripe patterns, leading to oblique or rectangular patterns.

In two dimensions the prestructure can also be oriented differently, e.g., perpendicular to the meniscus. We consider a prestructure of the form

$$m(\mathbf{x}) = \tanh\left\{10\left[4\left|\text{frac}\left(\frac{y}{L_{\text{pre}}}\right) - 0.5\right| - 1\right]\right\}. \quad (9)$$

The transferred patterns are shown in Fig. 10. In this case a large variety of qualitative different structures can be generated depending on the transfer velocity v and prestructure contrast ρ. For low velocities ($v = 0.022, \rho = 0.001$), stripes perpendicular to the meniscus are formed, just like in the case of a homogeneous substrate, but with wavelengths that have a fixed 2:1 ratio to the wavelength of the prestructure ($L_{\text{pre}} = 200$). For increased velocities ($v = 0.028$), stripes that are slightly tilted against the prestructure are created. There the prestructure wavelength or a commensurable ratio of it is not a favorable wavelength for the system. Therefore, the system effectively changes the wavelength by tilting the stripes, similar to the Benjamin-Feir instability mechanism leading to the zigzag pattern in other pattern-forming systems [45], while reacting to the prestructure with the y component of the wave vector. In the case of $v = 0.028, \rho = 0.002$, the y component exhibits a 4:1 locking, which can be best seen by looking at the Fourier transform of the pattern (see Fig. 11, right panel). While the tilt angle is defined by the ratio of the wavelength the system favors and the wavelength introduced by the prestructure, the tilt direction (to the left or the right) is determined by the initial conditions and is sensitive to slight perturbations.

Further increased velocities lead to more complex pattern topologies. For $v = 0.034$, lattice structures of small domains in the LC phase are created, where each row is shifted horizontally by half a wavelength with respect to the previous row. For higher velocities, this does not hold true and the LC domains of the patterns are no longer regular, resulting in irregular looking patterns. However, for some parameter sets, quite regular rows consisting of irregular domains can be identified, e.g., for $v = 0.046, \rho = 0.002$. For high velocities near the upper boundary of the patterning regime, fully regular patterns arise again. They consist of domains that are well aligned in rows and columns and are locked to the prestructure. They can be understood as a superposition of the natural pattern in the absence of a prestructure, which are stripes parallel to the meniscus and the perpendicular stripe pattern induced by the prestructure.

A comparison of Figs. 9 and 10 exhibits completely different behavior of the patterning process, only depending on the orientation of the prestructure. This reveals the different nature of the two basic pattern types on homogeneous substrates,

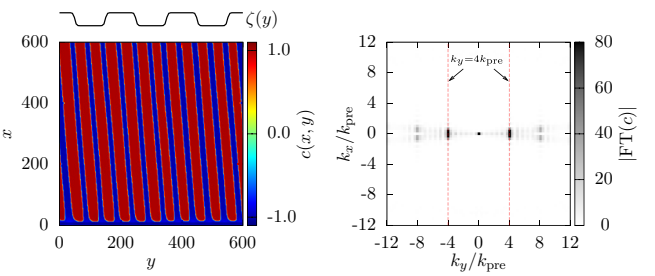

FIG. 11. (Color online) Oblique stripe pattern arising on a vertically prestructured substrate ($L_{\text{pre}} = 200, v = 0.028, \rho = 0.002$) and its Fourier transform. The dominant Fourier modes are integer multiples of the wave number k_{pre} of the prestructure.

which are stripes parallel and perpendicular to the meniscus. Stripes perpendicular to the meniscus occur as a result of a secondary instability, after stripes parallel to the meniscus have been formed [26]. Therefore, this instability might be suppressed more easily by a corresponding prestructure (see Fig. 9) than the instability leading to stripes parallel to the meniscus. This could explain the various patterns shown in Fig. 10, which might result from a competition between the strong tendency to form stripes parallel to the meniscus for high transfer velocities and the prestructure that favors stripes perpendicular to the meniscus.

Notice that a comparison with results for other spatially forced pattern-forming systems [10,12] reveals interesting similarities, such as the formation of complex two-dimensional oblique and lattice patterns as a result of a one-dimensional spatial forcing. This is notable, as Cahn-Hilliard models generally have no intrinsic critical wave number, in contrast to the systems studied in [10,12]. However, in the case described here, the transfer process included in the Cahn-Hilliard model acts as a wave-number selection mechanism, leading to the noticeable similarities to the aforementioned systems.

VI. CONCLUSION AND OUTLOOK

A theoretical investigation of Langmuir-Blodgett transfer onto prestructured substrates by means of a generalized Cahn-Hilliard model has been presented. Starting with the one-dimensional case, we found locking effects of different order with periodic prestructures. Utilizing these effects, the patterning process can be controlled more precisely, patterns of higher complexity can be obtained, and the patterning regime can be extended to a larger control parameter range.

In the two-dimensional case, prestructured substrates can be used to stabilize the production of stripes parallel to meniscus, as well as to enable a variety of different complex patterns, if the prestructure orientation is changed. Again, locking effects enable an additional control mechanism over the patterning process. This concept might be extended to similar systems, such as orientation control in a quenched system [43].

Towards a more detailed understanding of the processes in the real experiments one should further investigate the legitimacy of the assumptions made in the derivation of the Cahn-Hilliard model used here, in the case of prestructured substrates. The approximation of a static meniscus might become improper for prestructures, which introduce a wettability contrast and therefore influence the dynamics of the meniscus. This falls outside the scope of this paper and is left for future work.

ACKNOWLEDGMENTS

This work was supported by the Deutsche Forschungsgemeinschaft within SRF TRR 61. We thank Michael H. Köpf, Lifeng Chi, and Uwe Thiele for fruitful discussions. We also gratefully acknowledge many fruitful discussions with the late Dr. Rudolf Friedrich.

[1] L. Glass, Nature (London) **410**, 277 (2001).
[2] A. Pikovsky, M. Rosenblum, and J. Kurths, *Synchronization: A Universal Concept in Nonlinear Sciences* (Cambridge University Press, Cambridge, 2003).
[3] T. Sugawara, M. Tachikawa, T. Tsukamoto, and T. Shimizu, Phys. Rev. Lett. **72**, 3502 (1994).
[4] S. Kaka, M. R. Pufall, W. H. Rippard, T. J. Silva, S. E. Russek, and J. A. Katine, Nature (London) **437**, 389 (2005).
[5] G. Filatrella, A. H. Nielsen, and N. F. Pedersen, Eur. Phys. J. B **61**, 485 (2008).
[6] M. Dolnik, T. Bánsági, S. Ansari, I. Valent, and I. R. Epstein, Phys. Chem. Chem. Phys. **13**, 12578 (2011).
[7] M. Lowe, J. P. Gollub, and T. C. Lubensky, Phys. Rev. Lett. **51**, 786 (1983).
[8] J. H. McCoy, W. Brunner, W. Pesch, and E. Bodenschatz, Phys. Rev. Lett. **101**, 254102 (2008).
[9] G. Freund, W. Pesch, and W. Zimmermann, J. Fluid Mech. **673**, 318 (2011).
[10] S. Rüdiger, D. G. Míguez, A. P. Munuzuri, F. Sagués, and J. Casademunt, Phys. Rev. Lett. **90**, 128301 (2003).
[11] P. Coullet, Phys. Rev. Lett. **56**, 724 (1986).
[12] R. Manor, A. Hagberg, and E. Meron, Europhys. Lett. **83**, 10005 (2008).
[13] A. P. Krekhov and L. Kramer, Phys. Rev. E **70**, 061801 (2004).
[14] A. Krekhov, Phys. Rev. E **79**, 035302 (2009).
[15] F. C. Krebs, Sol. Energ. Mat. Sol. C. **93**, 394 (2009).
[16] L. Li, M. H. Köpf, S. V. Gurevich, R. Friedrich, and L. Chi, Small **8**, 488 (2012).
[17] J. D. Swalen, D. L. Allara, J. D. Andrade, E. A. Chandross, S. Garoff, J. Israelachvili, T. J. McCarthy, R. Murray, and R. F. Pease, Langmuir **3**, 932 (1987).
[18] C. D. Dimitrakopoulos and D. J. Mascaro, IBM J. Res. Dev. **45**, 11 (2001).
[19] A. Bolognesi, C. Botta, and S. Yunus, Thin Solid Films **492**, 307 (2005).
[20] X. Chen, S. Lenhert, M. Hirtz, N. Lu, H. Fuchs, and L. Chi, Acc. Chem. Res. **40**, 393 (2007).
[21] H. Gau, S. Herminghaus, P. Lenz, and R. Lipowsky, Science **283**, 46 (1999).
[22] D. Qin, Y. Xia, B. Xu, H. Yang, C. Zhu, and G. M. Whitesides, Adv. Mater. **11**, 1433 (1999).
[23] K. M. Chen, X. Jiang, L. C. Kimerling, and P. T. Hammond, Langmuir **16**, 7825 (2000).
[24] A. Checco, O. Gang, and B. M. Ocko, Phys. Rev. Lett. **96**, 056104 (2006).
[25] M. H. Köpf, S. V. Gurevich, and R. Friedrich, Phys. Rev. E **83**, 016212 (2011).
[26] M. H. Köpf, S. V. Gurevich, R. Friedrich, and U. Thiele, New J. Phys. **14**, 023016 (2012).
[27] K. B. Blodgett, J. Am. Chem. Soc. **57**, 1007 (1935).
[28] M. Gleiche, L. F. Chi, and H. Fuchs, Nature (London) **403**, 173 (2000).
[29] K. Spratte, L. F. Chi, and H. Riegler, Europhys. Lett. **25**, 211 (1994).
[30] H. Riegler and K. Spratte, Thin Solid Films **210**, 9 (1992).
[31] K. Graf and H. Riegler, Colloids Surf. A **131**, 215 (1998).

[32] K. Spratte and H. Riegler, Langmuir **10**, 3161 (1994).
[33] A. Oron, S. H. Davis, and S. G. Bankoff, Rev. Mod. Phys. **69**, 931 (1997).
[34] R. V. Craster and O. K. Matar, Rev. Mod. Phys. **81**, 1131 (2009).
[35] O. K. Matar and S. M. Troian, Phys. Fluids **9**, 3645 (1997).
[36] M. H. Köpf, S. V. Gurevich, R. Friedrich, and L. Chi, Langmuir **26**, 10444 (2010).
[37] A. Novick-Cohen and L. A. Segel, Physica D **10**, 277 (1984).
[38] J. W. Cahn and J. E. Hilliard, J. Chem. Phys. **28**, 258 (1958).
[39] NVIDIA, CUDA C Programming Guide Version 4.2, 2013, http://docs.nvidia.com/cuda/cuda-c-programming-guide.
[40] M. H. Köpf and U. Thiele, Nonlinearity **27**, 2711 (2014).
[41] U. Thiele and E. Knobloch, Phys. Rev. Lett. **97**, 204501 (2006).
[42] U. Thiele, L. Brusch, M. Bestehorn, and M. Bär, Eur. Phys. J. E **11**, 255 (2003).
[43] V. Weith, A. Krekhov, and W. Zimmermann, Eur. Phys. J. B **67**, 419 (2009).
[44] See Supplemental Material at http://link.aps.org/supplemental/10.1103/PhysRevE.90.042926 for a movie of an exemplary simulation.
[45] M. C. Cross and P. C. Hohenberg, Rev. Mod. Phys. **65**, 851 (1993).